

What can be learned from the historical trend of crude oil prices? An ensemble approach for crude oil price forecasting



Mingchen Li ^{a,b}, Zishu Cheng ^{a,b}, Wencan Lin ^{a,b}, Yunjie Wei ^{a,c,*}, Shouyang Wang ^{a,c}

^a Academy of Mathematics and Systems Science, Chinese Academy of Sciences, Beijing 100190, China

^b School of Mathematical Sciences, University of Chinese Academy of Sciences, Beijing 100190, China

^c Center for Forecasting Science, Chinese Academy of Sciences, Beijing 100190, China

ARTICLE INFO

Keywords:

Crude oil price forecasting
Decomposition
Trajectory similarity
Machine learning

ABSTRACT

Crude oil price series are nonlinear and highly volatile, making it difficult to obtain satisfactory performance for traditional statistical-based forecasting methods. To improve forecasting accuracy, this study proposes a novel learning paradigm by integrating the trajectory similarity method with machine learning models based on the decomposition-ensemble framework. In the proposed learning paradigm, raw data of international crude oil prices are first decomposed using variational mode decomposition (VMD), after which, using sample entropy (SE), the resulting essential modal functions are divided into high and low frequencies. The process aims to reorganize the data by using the forecasting properties of different models. Finally, to obtain the final forecasting results, two models, i.e., the trajectory similarity method (TS) and long short term memory neural network (LSTM), are applied to predict and sum up the low and high-frequency subseries, respectively. As sample data for validation, this study selected the international crude oil price series of West Texas Intermediate (WTI) and Brent. Experimental results showed that the proposed VMD-SE-TS/LSTM learning paradigm significantly outperforms all other benchmark models, including the single models without decomposition and the hybrid models with decomposition. The proposed approach performs best in different evaluation metrics and statistical tests under different horizons, indicating that the proposed VMD-SE-TS/LSTM learning paradigm is effective and robust in crude oil price forecasting.

1. Introduction

With crude oil a pivotal energy source worldwide, meeting almost two-thirds of global energy needs and having an irreplaceable role in certain production processes (Karasu et al., 2020; Ma et al., 2018; Zhao et al., 2018), it is well recognized that the international crude oil price is of great concern to governments because of its impact on business, national security, energy conservation and emissions reduction (Karasu et al., 2020; Lu et al., 2020; Ratti and Vespiagnani, 2016; Tang et al., 2020; Yu et al., 2019). Accurate oil price forecasts also give managers, investors, and practitioners information for making decisions that maximize profits and minimize risk (Chai et al., 2018; Godarzi et al., 2014; Li et al., 2021; Wang et al., 2017).

Price fluctuations in crude oil are triggered not only by global political events but also by other events in financial futures markets, which leads to the price' nonlinear, highly volatile characteristics (Charles and Darné, 2017; Qadan and Nama, 2018; Teterin et al., 2016; Zhang et al., 2008). In light of this, much effort has been expended on inventing forecasting models or data processing algorithms to address the difficulty of capturing trends in nonlinear series (Jammazi and Aloui, 2012). Research on crude oil forecasting has received attention from researchers year on year, as shown in Fig. 1, and the number of relevant publications and citations has increased in recent years.

Forecasting researchers have considerable interest in a new combinatorial method, dubbed 'decomposition and ensemble' (Tang et al., 2020; Wu et al., 2019; Yu et al., 2014, 2015). That decomposes the original time series data into intrinsic mode functions, which are then regressed separately by the forecasting model and weighted to obtain prediction results. The validity and excellence of this approach have been shown across several areas, including crude oil prices, tourism demand, and gold prices (Bergmeir et al., 2016; Risse, 2019; Tang et al., 2018; Zhang et al., 2021). This study utilized a nonrecursive signal decomposition approach, variational mode decomposition (VMD), successfully avoid the modal mixing problem compared to the most

* Corresponding author at: Academy of Mathematics and Systems Science, Chinese Academy of Sciences, Beijing 100190, China.

E-mail address: weiyunjie@amss.ac.cn (Y. Wei).

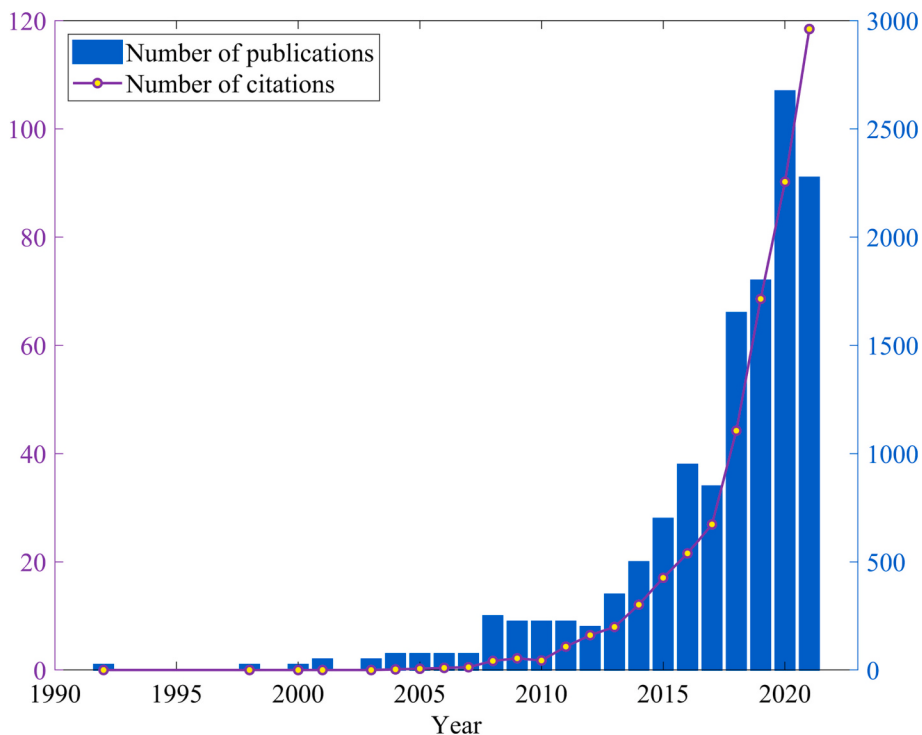


Fig. 1. Rising trend in publications and citations on crude oil price forecasting over 30 years.

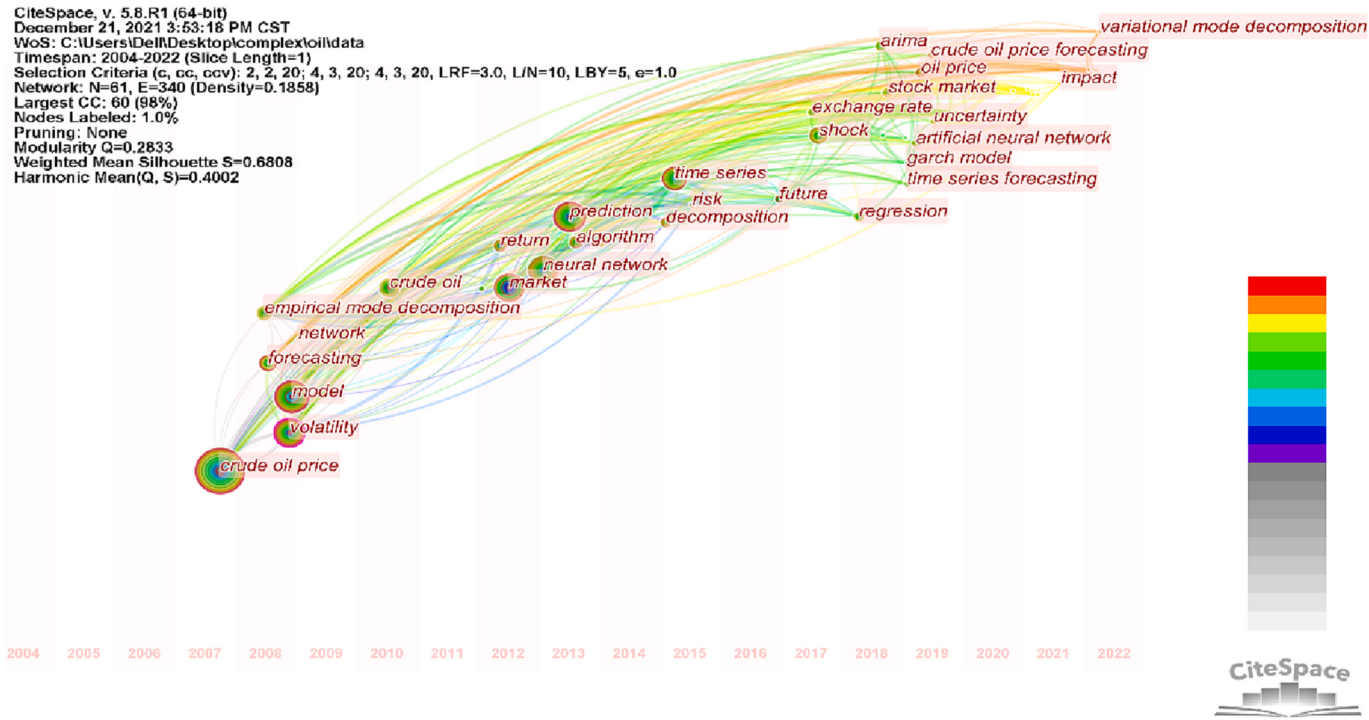


Fig. 2. Research hotspots in the literature on crude oil price forecasting.

prevalent method, empirical mode decomposition (EMD) (Dragomir-etskiy and Zosso, 2014; Zhang et al., 2008). The decomposed subsequence that results contains flatter trend terms and more volatile short-term impact components or noise components, and it corresponds to the trajectory similarity method (TS) and long short term memory neural network (LSTM, a kind of artificial neural networks) models' relative forecasting advantages. As shown in Fig. 2, decomposition algorithms

were applied to crude oil price forecasting as early as 2008, and VMD also appeared in crude oil forecasting around 2021 (Chen, 2004).

The two main research methods used in conducting oil price volatility analysis and oil price forecasting are the univariate or multivariate analysis of forecasts and artificial intelligence-based forecasting (Dra-chal, 2016; Miao et al., 2017; Mohammadi and Su, 2010; Wang et al., 2016). Based on traditional econometrics, the advantage of the first

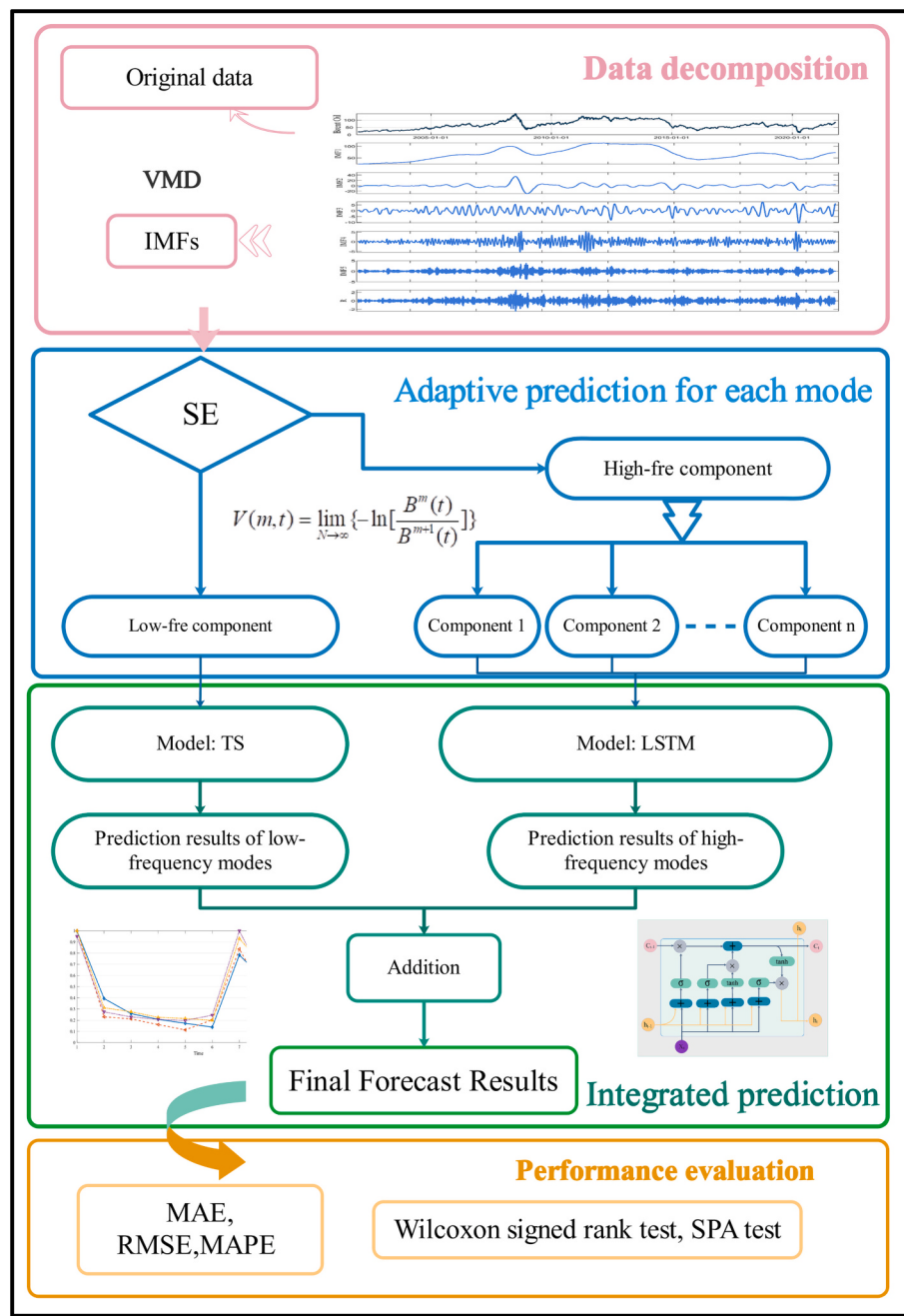


Fig. 3. Framework for this study.

method is that it is supported by solid economic theory for modeling and, to a certain extent, by better causal explanations. However, it has relatively poor forecasting accuracy (Lu et al., 2020). The second method, artificial intelligence-based forecasting, which includes machine learning and deep learning (artificial neural networks, ANNs) (Ghodousi et al., 2019; Godarzi et al., 2014; Wang et al., 2018b; Xiong et al., 2013), has been widely used in recent studies because it is an effective with nonlinear data and does not require assumptions of stability and distribution (Lecun et al., 2015; Miao et al., 2017; Zhao et al., 2017; Luo et al., 2019). Since artificial intelligence methods, mainly data-driven to make predictions, are internally like 'a black box', the method lacks interpretability. For low-frequency series or trend items, using this method is inappropriate if predictions and interpretations of trends are the priority (Wang et al., 2020; Zhang et al., 2020; Zhao et al., 2017). As shown in Fig. 2, traditional models such as ARIMA and models

such as neural networks both maintain a place in the field of predicting crude oil prices.

In response to the shortcomings of ANN, regarding the treatment of trend term forecasts and interpretability, identifying the similarity of time series may be an effective and robust means. By utilizing a similarity algorithm (such as trajectory similarity, TS), one can determine the similarity of different time series, ascertain the relationship between different series, and conduct research on classification, clustering and forecasting. The similarity measure of time series has been widely applied in traffic flow, speech recognition, finance, tourism, and other time series (D'Urso et al., 2021; Dehak et al., 2011; Li, 2021; Xiao et al., 2020). For example, when international crude oil prices plunged near March 4, 2020 in response to inconclusive OPEC+ negotiations, unpredictable results were produced; but, near May 1, 2017, and near December 21, 2004, crude oil prices experienced similar plunges and

rebounds, the correlation of which can then be disposed of in accordance with TS (see [Section 3](#) for details). This study applies similarity of time series for the first time in crude oil price forecasting to its interpretation to support forecasting and decision making. LSTM have excellent nonlinear series forecasting capability ([Wu et al., 2019](#)). Since each of these two models has distinct features, combining their strengths may improve forecasting outcomes. The decomposed IMFs should be tailored to various forecasting methodologies due to their varying frequencies ([Li et al., 2020](#)). This study, therefore, combines both types of models, TS and LSTM, in terms of model use to achieve better forecasting accuracy and then validates it in empirical evidence.

The VMD-SE- TS/LSTM approach based on modal frequencies for crude oil price forecasting is proposed by this study to overcome the difficulty of nonlinearity and high volatility of crude oil prices series. First, we use variational mode decomposition (VMD) to decompose the original crude oil price series into different IMFs. Second, we calculate the complexity of various IMFs using sample entropy (SE). Third, we assign different forecasting models according to the SE value, i.e., using TS for low-frequency series and LSTM for high-frequency series. Finally, the forecasting results of each IMF are summed and compared with the benchmark model results for error evaluation and statistical test analysis. The superiority of this approach stems from three factors: 1) decomposition methods for nonlinear sequences, 2) the combination of an explanatory TS model with an LSTM capable of handling high-frequency data, 3) using trajectory similarity, time series windows of similar volatility in history can be obtained to guide the improvement of prediction accuracy, especially in the case of critical emergencies.

Based on the considerations above, this paper's contributions mainly include three aspects: First, the trajectory similarity method is used for the first time for crude oil price forecasting. Based on an extremely rich library of series, TS can find traces of the present in historical patterns and make accurate trend judgments and reliable series forecasts. Second, time complexity calculation is used to divide decomposed subsequences (i.e., IMFs). The subseries processed by the decomposition algorithm reflect the trends in different modes with different volatility and frequency, and should be disposed of separately and appropriately. Third, the study offers separate forecasting strategies for trend variables and highly volatile variables. Considering the characteristics of time series and the advantages of forecasting models, new insights into crude oil price forecasting can be discovered when TS is used to forecast low-frequency series while LSTM is used to forecast high-frequency series.

The remainder of the paper is laid out as follows: [Section 2](#) introduces the research framework, decomposition method and forecasting models; [Section 3](#) describes the entire experimental procedure and assesses the proposed model's performance using two types of empirical evidence, which are error evaluation and robustness testing; and [Section 4](#) concludes and discusses future research directions.

2. Methodology

This section will first give the framework of the study and detail the steps involved; afterward, the algorithms that appear in the framework will be introduced, including decomposition algorithms, time series complexity calculation methods and forecasting models.

2.1. Research framework

The forecasting approach this study propose aims to improve crude oil price forecasting's accuracy after extracting information about different modes from oil price series data using decomposition methods and then assigning appropriate forecasting methods to the different modes. Accurate forecasting results will provide guidance for trading strategies and policy measures of crude oil futures market management. The study's framework shown in [Fig. 3](#) has four main stages:

Stage 1: data decomposition. We collect two informative sets of crude oil price series, the Brent and WTI, and later decompose the

original crude oil price series Y into IMF_i ($i > 2$) using the VMD algorithm.

Stage 2: Adaptive prediction for each mode. We first compute the time complexity (i.e., sample entropy) for each component IMF_i and assign different models (TS and LSTM) to them based on their results.

Stage 3: Integrated prediction. This stage consists of two main steps, individual forecasting for each IMF using the corresponding method, and final forecasting, in which individual forecasts are linearly combined to obtain the final results.

Stage 4: Performance evaluation. Three commonly used evaluation criteria, MAE, RMSE and MAPE, are used to compare predictive performance. Two valid statistical tests, namely Wilcoxon signed rank test and superior prediction ability test (SPA), are used to statistically compare the models' accuracy in crude oil price forecasting. Multi-step ahead forecasting is also included in the assessment framework.

2.2. Related methods

2.2.1. Variational mode decomposition

By generating and solving variational problems, variational mode decomposition (VMD) can decompose raw time series data into a finite number of intrinsic mode functions (IMFs) ([Dragomiretskiy and Zosso, 2014](#)). The algorithm transforms the original sequence into an adaptively determined correlation band w_k and into several modes u_k with different band limits to equalize errors between modes. The specific calculation process is:

First, each IMF (i.e., $r_k(t)$) is treated as an AM-FM signal (AM-FM: amplitude modulated-frequency modulated).

Second, the center frequency of each analyzed signal is calculated, and the spectrum of each mode signal is tuned to the corresponding 'baseband'.

Third, the bandwidth of each IMF is determined using the demodulated signal's H^{-1} Gaussian smoothness, and the constrained variational problem can be transformed into dealing with the optimization problem as follows:

$$\min_{\{r_k, \omega_k\}} = \left\{ \sum_k \left\| \partial_t \left[\left(\delta(t) + \frac{j}{\pi t} \right)^* r_k(t) \right] e^{-j\omega_k t} \right\|_2^2 \right\} \\ \text{s.t. } \sum_k r_k = y_t, \quad (1)$$

Lagrangian multipliers λ are used to transform the above constraint variation problem into the following unconstrained problem:

$$L(\{u_k\}, \{\omega_k\}, \lambda) = \\ \alpha \sum_k \left\| \partial_t \left[\left(\delta(t) + \frac{j}{\pi t} \right)^* r_k(t) \right] e^{-j\omega_k t} \right\|_2^2 + \\ \left\| y_t - \sum_k r_k(t) \right\|_2^2 + \left\langle \lambda(t), y(t) - \sum_k r_k(t) \right\rangle, \quad (2)$$

where α is the quadratic penalty factor, $\lambda(t)$ denotes the Lagrange multiplier, u_k represents band-limited modes, and w_k is the adaptively determined relevant bands. For the specific solution process, refer to ([Dragomiretskiy and Zosso, 2014](#); [Li et al., 2020](#)).

2.2.2. Sample entropy

Sample entropy (SE) is an excellent tool to measure the complexity of time series data, and has been popularly introduced in signal processing ([Pham and Yan, 2018](#)). Widely used because of its excellent estimation ability and anti-interference ability, it can utilize a small quantity of data to obtain robust estimates and is convenient for processing mixed time series.

Calculation includes the following six steps:

1) Recombine sequence Y into a matrix:

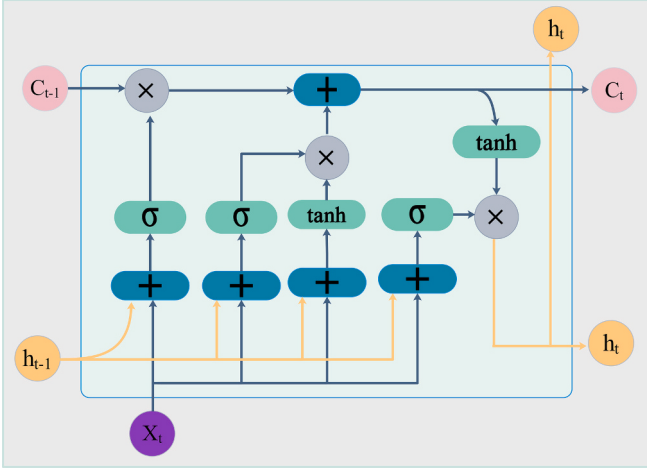


Fig. 4. The structure of the LSTM.

$$Y = \begin{bmatrix} y(1) & y(2) & \dots & y(N-m+1) \\ y(2) & y(3) & \dots & y(N-m+2) \\ \vdots & \vdots & \ddots & \vdots \\ y(m) & y(m+1) & \dots & y(N) \end{bmatrix} \quad (3)$$

2) The distance between two vectors is defined as follows:

$$d[y(i), y(j)] = \max(|y(i+1) - y(j+1)|), \quad (4)$$

$(1 \leq i \leq m-1; 1 \leq j \leq N-m+1)$

where l represents the step length.

3) For the fixed condition $d[y(i), y(j)] \leq t$, there are a threshold t and a note B_i as the number to meet. After that, the ratio $Bm_i(t)$ can be computed with:

$$Bm_i(t) = \frac{1}{N-m+1} B_i \quad (5)$$

4) Compute the mean of the ratio $Bm(t)$:

$$Bm(t) = \frac{1}{N-m} \sum_{i=1}^{N-m} Bm_i(t) \quad (6)$$

5) Repeat stages 1 to 3 and update; afterward, obtain $B^{m+1}(t)$:

$$B^{m+1}(t) = \frac{1}{N-m} \sum_{i=1}^{N-m} B^{m+1}_i(t) \quad (7)$$

6) The value of sample entropy is calculated:

$$V(m, t) = \lim_{N \rightarrow \infty} \left\{ -\ln \left[\frac{B^m(t)}{B^{m+1}(t)} \right] \right\} \quad (8)$$

2.2.3. Long short term memory neural network (LSTM)

The long short term memory neural network (LSTM), which is derived on the recurrent neural network (RNN), is designed for long-term dependency learning. Fig. 4 depicts the structure of LSTM, and its implementation comprises of four stages.

Stage 1. Forget gate: deciding which part of the information is forgotten from the cell state C_{t-1} .

$$f_t = \sigma(W_f \cdot [h_{t-1}, x_t] + b_f) \quad (9)$$

where W_f and b_f are the weight matrix and bias vector of the threshold f_t (a value between 0 and 1), respectively. h_{t-1} and x_t represent the hidden state at the last time step and the input at the current time step, respectively.

Stage 2. Determines which data may be saved in the cell state. This process consists of two phases:

$$i_t = \sigma(W_i \cdot [h_{t-1}, x_t] + b_i) \quad (10)$$

$$\hat{C}_t = \tanh(W_C \cdot [h_{t-1}, x_t] + b_C) \quad (11)$$

where W_i and W_C , b_i and b_C are the weight matrix and bias vector of i_t and \hat{C}_t , respectively.

Stage 3. Update the cell status for the current time step C_t .

$$C_t = f_t^* C_{t-1} + i_t^* \hat{C}_t \quad (12)$$

Stage 4. Obtain the output of the LSTM module. This process consists of two phases:

$$o_t = \sigma(W_o \cdot [h_{t-1}, x_t] + b_o) \quad (13)$$

$$h_t = o_t^* \tanh(C_t) \quad (14)$$

where W_o and b_o are the weight matrix and bias vector of the threshold o_t , respectively. The final output is obtained by the change of h_t .

2.2.4. Trajectory similarity

For the correlation of the current time series with past periods, we use the trajectory similarity method to find the closest traces from the historical data, with the following detailed calculation steps.

In the first step, we need to divide the time windows and normalize the data for each time window:

$$x^* = \frac{x - \min(X)}{\max(X) - \min(X)} \quad (15)$$

where X represents the sequence values throughout the time window, x represents the original value and x^* is the normalized value.

In the second step, the similarity is calculated, and the sequence with the best similarity match is found:

$$\min\{DTW(S_t, S_n)\}, n = 1, 2, \dots, t-1 \quad (16)$$

where DTW stands for the method of calculating similarity, i.e., dynamic time warping, which we explain in the next section, and S_t stands for the time window at time t .

In the third step, we make a prediction based on the actual value of the succession of historical data series with the best similarity.

2.2.5. Dynamic time warping

The core of the trajectory similarity approach is the choice of metric for determining similarity, and previous research has shown that dynamic time warping (DTW) is a robust method for measuring similarity between two time series (Li, 2021; Zhao and Itti, 2018). DTW allows time points with the same shapes at different times. The warping alignments enable DTW to measure the similarity between time series with unequal lengths. Moreover, the obtained distance is not sensitive to abnormal points (Kim et al., 2018).

First, assume that there are two time series $T = \{t_1, t_1, \dots, t_n\}$ and $S = \{s_1, s_1, \dots, s_m\}$ (in this study, the time window to be predicted versus the time window of historical data). Then DTW can be expressed as:

$$DTW(S, T) = \mathbf{R}(m, n) = \min_{\mathbf{R}} \sum_{k=1}^K d(i_k, j_k) \quad (17)$$

where \mathbf{R} is the cost matrix, namely, the accumulated distance matrix; $\mathbf{R}(m, n)$ denotes the cell value at the intersection of the n -th row and the m -th column in the cost matrix \mathbf{R} and is the minimal distance returned by DTW. As \mathbf{R} is the accumulated distance matrix, $\mathbf{R}(m, n)$ is the sum of all the sub-distances between two time points that comprise the k -th element P_k of the optimum warping path $P = \{p_1, p_2, \dots, p_k\}, k \in [1, K]$ (To determine the best distance between trajectories S and T , a path created across the distance matrix must minimize the cumulative distance between them; this path is referred to as the twisted path). The best

Table 1
The parameters of the forecasting models.

Model	Parameters	Determination approach	Values
Snaïve ELM	Seasonal period	Preset	5
	Input dimension	Preset	–
	Number of hidden layer nodes	Trial and error approach	32
SVR	Output dimension	Preset	1
	Regularization coefficient c	Grid search	[1300]
	Kernel parameter g	Grid search	[2^{-5} , 2^5]
ANN &LSTM	Input dimension	Preset	–
	Number of hidden layer nodes	Trial and error approach	[32,64]
	Output dimension	Preset	1
	Training algorithms	Back propagation	–
	Initial learning rate	Trial and error approach	0.001
	Batch size	Trial and error approach	32
	Maximum of epochs	Preset	200

warping path found in the cost matrix \mathbf{R} is computed by:

$$\mathbf{R}(i,j) = d(i,j) + \min \begin{cases} \mathbf{R}(i,j-1) \\ \mathbf{R}(i-1,j-1) \\ \mathbf{R}(i-1,j) \end{cases} \quad (18)$$

where $d(i,j)$ denotes the subdistance between two time points.

2.2.6. Benchmark models and parameter settings

For comparison purposes, the five popular forecasting techniques in traditional econometrics methods and machine learning are employed as the crude oil price forecasting method, such as seasonal Naïve (Snaïve), extreme learning machine (ELM), support vector regression

(SVR), artificial neural networks (ANN) and LSTM. For detailed description of each model, refer to (Mohammadi and Su, 2010; Nademi and Nademi, 2018; Wang et al., 2018a; Weng et al., 2021). The models' parameter settings are listed in Table 1. Numpy, Pandas, Tensorflow and Keras packages are used in python 3.0 for model training and testing. And SVR is implemented by running libsvm in MATLAB 2018b.

3. Empirical studies

3.1. Data collection

Since they constitute a decisive factor in the configuration of prices of the most other commodities, are widely used as the basis of many crude oil formulas, and are the most famous benchmark prices, Brent crude oil price and West Texas Intermediate (WTI) crude oil price are the most famous benchmark prices, were chosen for our study (Jammazi and Aloui, 2012; Yu et al., 2008). The two crude oil price data used in this study are daily data.

Both datasets were acquired from the wind database (<http://www.wind.com>). The Brent dataset contained 5001 records from December 26, 2001 to October 19, 2021, excluding public holidays, while the WTI dataset had 4510 records from November 25, 2002 to October 19, 2021, excluding public holidays. These data series are divided into a training dataset, which covers the first 80% of the sample set, and a test dataset, which covers the remaining 20%. In addition, multistep ahead forecasts are made in the range of 1, 3 and 6 days to verify the model's robustness. The two sets of sequences are presented in Fig. 5, highlighting the dataset's considerable volatility and periodicity. By way of example, on April 20, 2020, the price of U.S. West Texas light crude oil futures (WTI) came out at the jaw-dropping closing of -\$37.63 per barrel, dipping as low as -\$40.31 per barrel at one point during the session. This highly unique situation is mainly due to global economic stagnation caused by



Fig. 5. International crude oil price data (Brent and WTI).

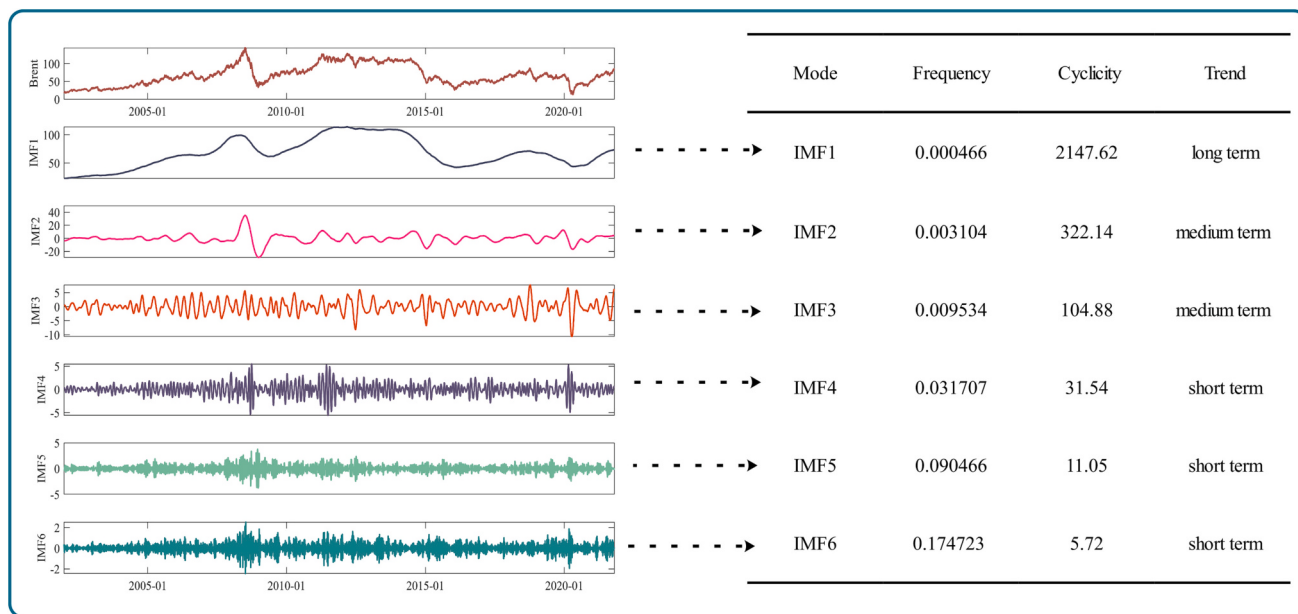


Fig. 6. Subseries of Brent international crude oil price data decomposed by VMD.

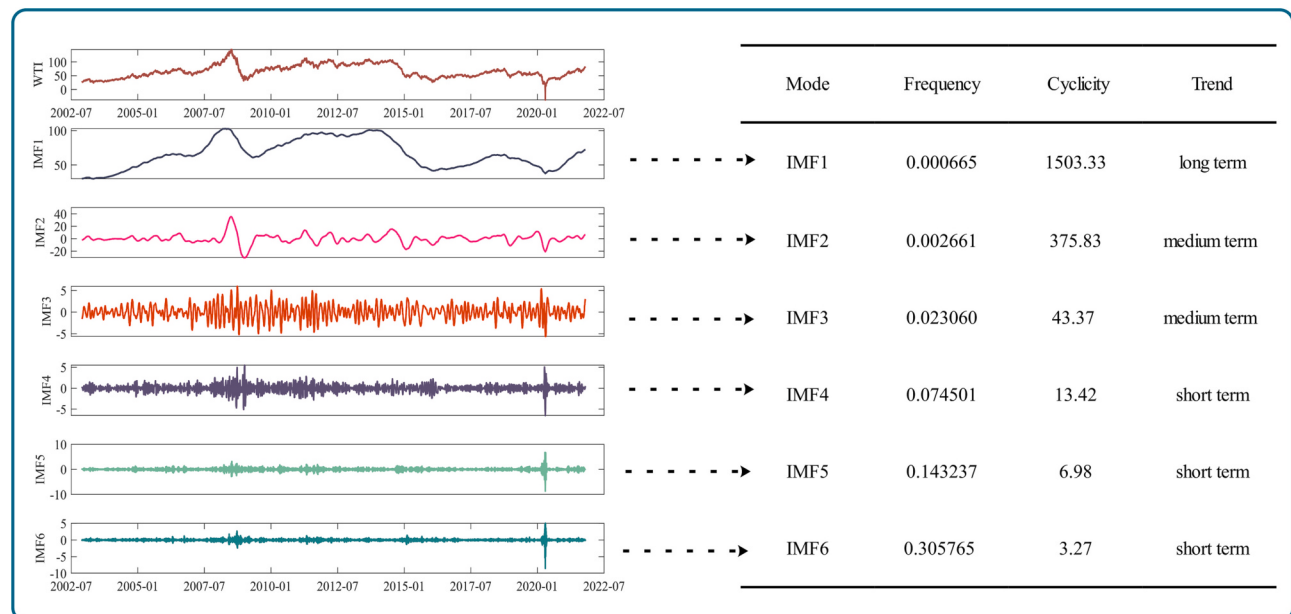


Fig. 7. Subseries of WTI international crude oil price data decomposed by VMD.

the COVID-19 epidemic, which led to a plunge in demand for crude oil with no takers to accept contracts that were soon to expire.

3.2. Data decomposition and adaptive prediction for each mode

After collecting the daily Brent and WTI crude oil prices, VMD was applied to decompose the original time series into several terms. Figs. 6–7, which illustrate decomposition results, show that the price time series of crude oil futures is decomposed into six intrinsic patterns, which were labeled IMF₁ to IMF_n (R), where IMF₁ represents the lowest frequency pattern, and IMF_n (R) represents the highest frequency pattern. The decomposed IMFs all exhibit different periodicity. As indicated in Fig. 7, the daily crude oil price is decomposed into six intrinsic modes (Take WTI as an example). The six intrinsic modes are denoted IMF₁ through IMF₆, with IMF₁ indicating the mode with the lowest frequency and

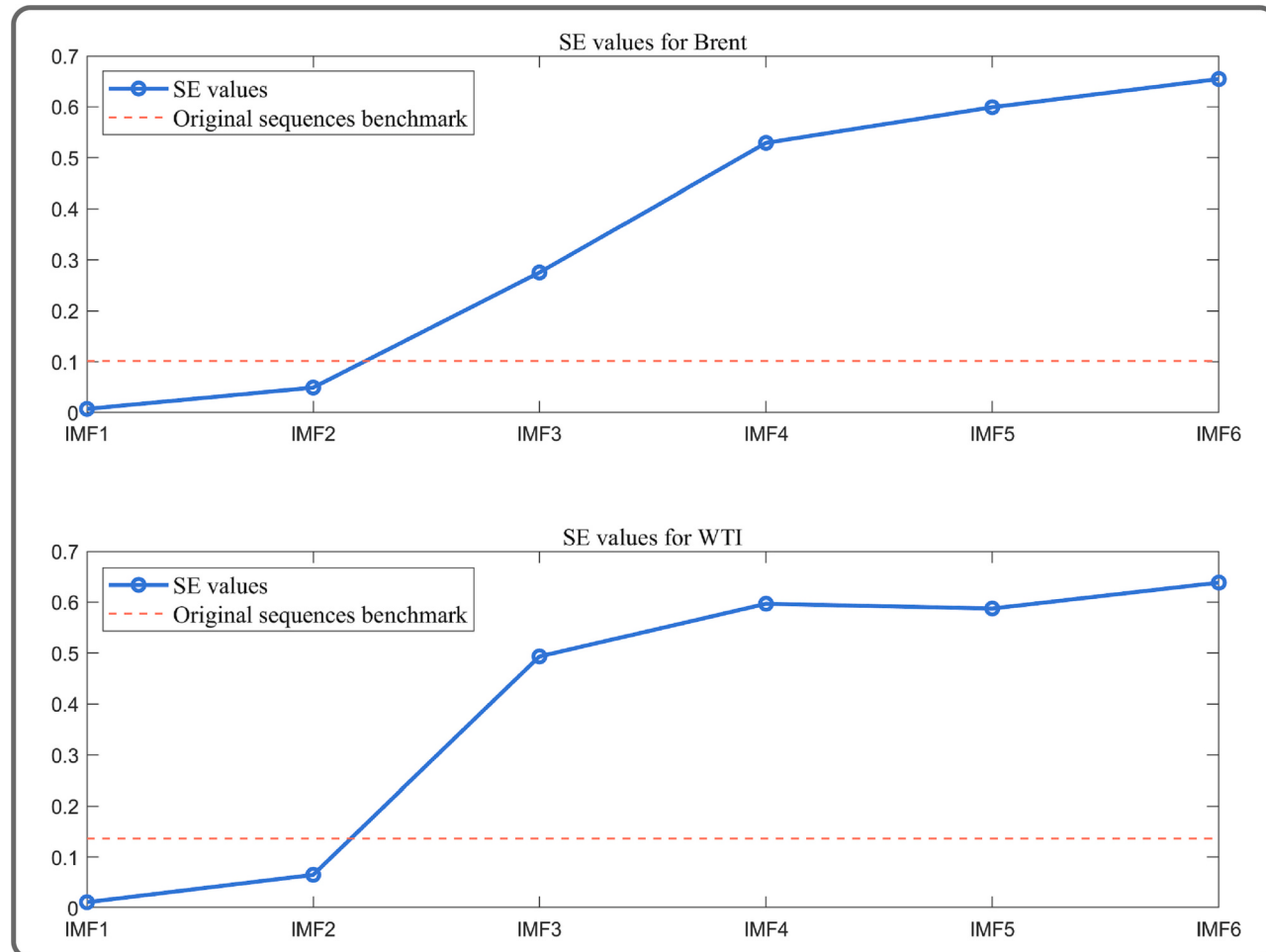
IMF₆ indicating the mode with the highest frequency. It is observable that each of the decomposed intrinsic modes has a distinct periodicity. For the oil price, the IMF₁ reflects the relative long-term trend of the time series, IMF₂–IMF₃ reflects the relative medium-term fluctuations and IMF₄–IMF₆ reflects the relative short-term fluctuations in the market. From the decomposition results, three pattern characteristics of the subsequence can be derived: periodicity, variability and tendency.

We use SE to calculate the different IMFs' entropy (degree of confusion, which also represents the frequency level). There are two methods in contemporary research about the distinguishing criteria: First, based on the rate of change. The researcher will determine which subsequences are closer based on the calculated SE values and the curves of the plotted SE, and then discriminate and reconstruct them (Wu and Lin, 2019; Zhao et al., 2022). Second, based on the SE values of the original sequences. The three categories of subsequences with SE values close to,

Table 2

The SE values of the original series and subseries.

	Original series	IMF1	IMF2	IMF3	IMF4	IMF5	IMF6
Brent	0.10133	0.00730	0.04921	0.27530	0.52925	0.59928	0.65468
WTI	0.13645	0.01139	0.06515	0.49347	0.59695	0.58760	0.63852

**Fig. 8.** Sample entropy of Brent and WTI components.

less than and greater than the SE value of the original sequence are distinguished (Zhang et al., 2014). In this study, the results obtained by these two methods were consistent. As shown in Table 2 and Fig. 8, there is a large variation from IMF2 to IMF3, and the value of SE of the original sequence lies in the middle of the two, so we choose the SE value of the original sequence as the distinguishing criteria in this study. By using LSTM for prediction of high-frequency IMFs and the TS model for forecasting of low-frequency IMFs, we intend to make reasonable use of the respective points of different types of forecasting models and subsequently achieve optimal forecasting results.

3.3. Evaluation indicators

To evaluate the point forecasting performance, three typical criteria, i.e., mean absolute percentage error (MAPE), root mean square error (RMSE) and mean absolute error (MAE), are adopted for this study. Formulas for calculating MAPE, RMSE, and MAE can be represented as:

$$MAPE = \frac{1}{N} \sum_{t=1}^N \left| \frac{y_t - \hat{y}_t}{y_t} \right|, \quad (19)$$

$$RMSE = \sqrt{\frac{1}{N} \sum_{t=1}^N (\hat{y}_t - y_t)^2}, \quad (20)$$

$$MAE = \frac{1}{N} |\hat{y}_t - y_t|, \quad (21)$$

where \hat{y}_t and y_t are the forecasted crude oil prices and the actual crude oil prices, and N denotes the size of the testing dataset.

Two tests, including the Wilcoxon signed rank test (WSRT) and the superior predictive ability (SPA) test, were conducted to provide statistical evidence of the model's predictive power. WSRT is a widely used, practical nonparametric inference test (Zhao and Itti, 2018; Zhao et al., 2017). Its null hypothesis is that the loss differential series has zero median, and the loss differential series is:

$$l(t) = f(e_A(t)) - f(e_B(t)) \quad (22)$$

where $f(*)$ represents the loss function (generally MSE). $e_A(t)$ and $e_B(t)$ represent the prediction error series of models A and B, respectively.

SPA, as a statistical test method for testing the superior predictive

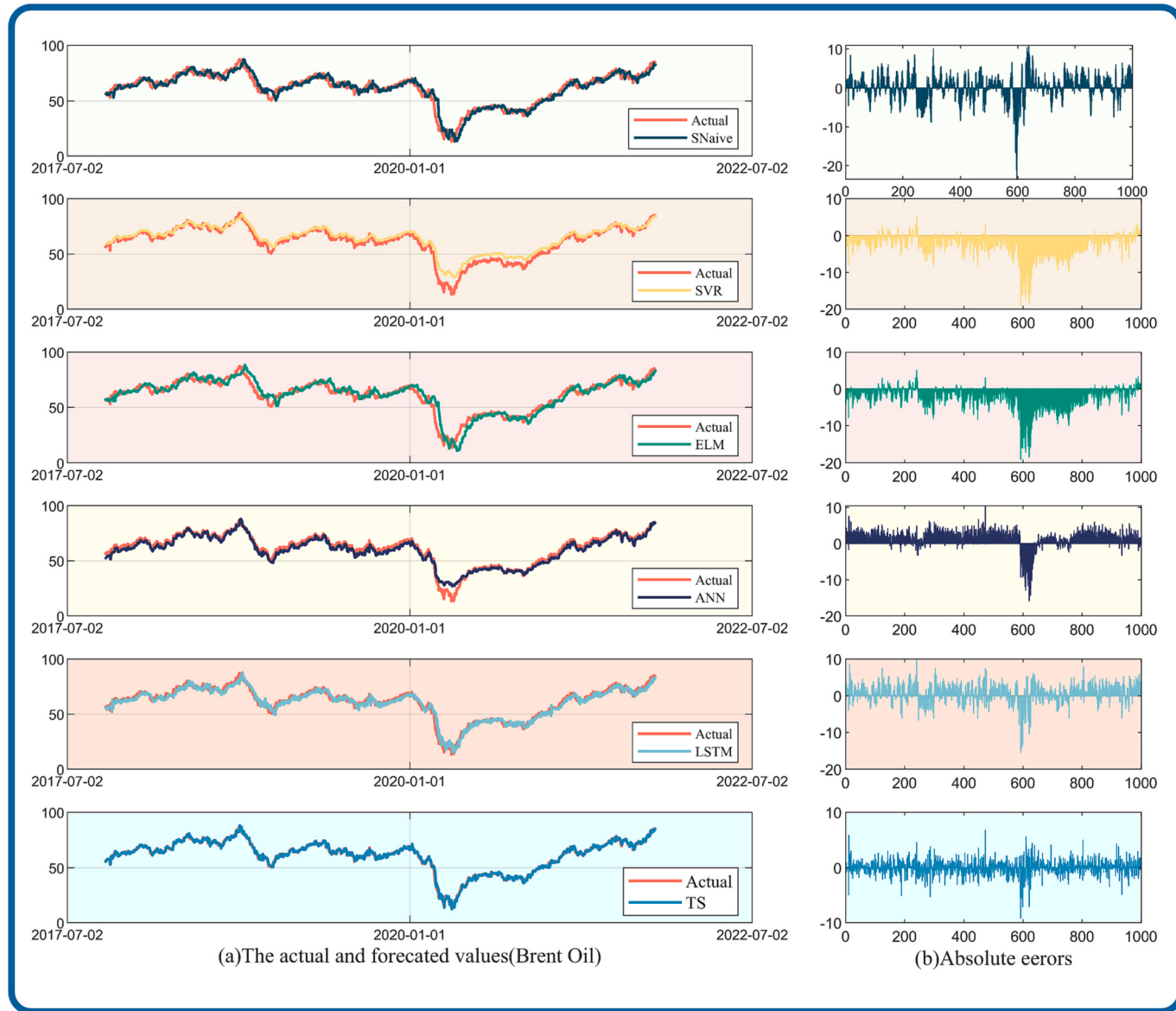


Fig. 9. The fitting performance with point-by-point error under one-step forecasting (Brent).

ability of point forecasting from a statistical perspective (Hansen, 2005), can test whether the accuracy performance of the target model is superior to other benchmark models through the model losses (MSE). The conclusion that the benchmark is the best is this null hypothesis:

$$H_0 : \max_i E[L_i] \geq E[L_{bm}] \quad (23)$$

where L_i represents MSE of the i th model, and L_{bm} is the MSE of the benchmark. For more information about the SPA test, refer to (Hansen, 2005).

3.4. Forecast results

In this section, we will evaluate the accuracy and robustness of the proposed model with error evaluation and statistical tests, respectively. The results of the benchmark models used are displayed accordingly for comparison, and the predictions of multiple horizons are taken into account.

3.4.1. Error evaluation

To assess our approach's predictive performance, we first build

benchmark models using a variety of the most commonly used predictive techniques to perform a single model performance comparison. For the single model performance comparison, we constructed several benchmark models using econometric-based methods, traditional machine learning methods, and deep learning methods, each using the same number of forecasting periods and time steps as our proposed approach. Benchmark models covered six types, Snaive, SVR, ELM, ANN (back propagation neural network in this study), LSTM and TS, and these models' performance in fitting point-by-point errors under single-step forecasting is given in Figs. 9–10. Their forecasting accuracy and ranking of forecasting methods are detailed in Tables 3–4.

When comparing the predicting performance of four single forecasting models across three different time steps, as shown in Tables 3–4, some striking observation to emerge from the data comparison. First, the model suggested for this study (i.e., TS) outperforms other models in forecasting crude oil prices, while taking MAPE for the Brent dataset as an example, the MAPE of TS model compared to Snaive, SVR, ELM, ANN and LSTM were reduced by 45.66%, 59.55%, 55.12%, 44.08% and 30.07, respectively. The data indicate that the TS model can significantly improve the forecasts' fitting performance, made possible by the

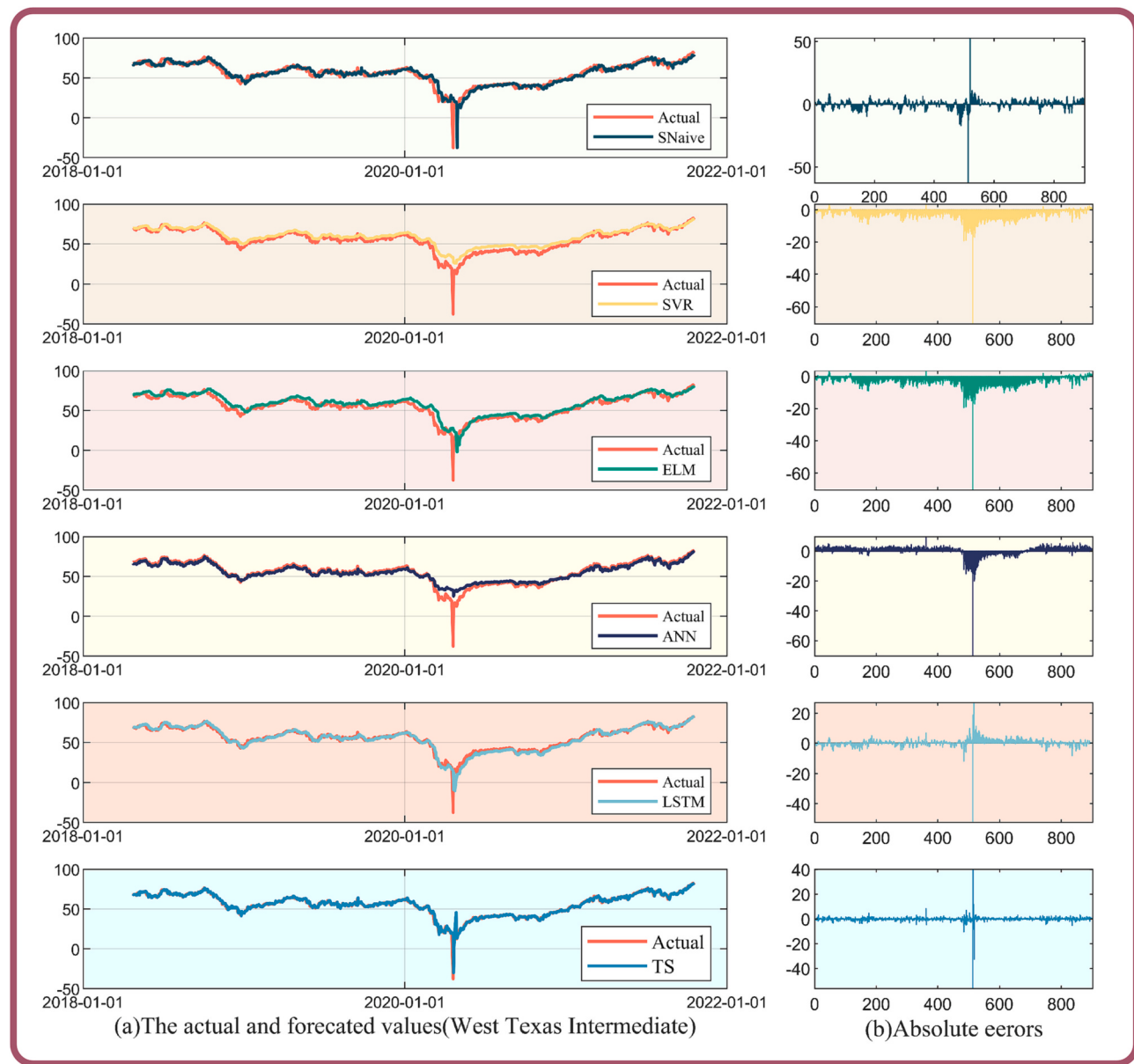


Fig. 10. The fitting performance with point-by-point error under one-step forecasting (WTI).

Table 3
Single model forecasting error (Brent).

Horizon	Indicators	Snaive	SVR	ELM	ANN	LSTM	TS
H = 1	MAE	3.46	3.20	2.69	2.60	2.28	1.61
	RMSE	4.72	4.33	4.29	3.24	2.92	1.97
	MAPE (%)	6.93	7.59	6.84	5.49	4.39	3.07
H = 3	MAE	–	3.10	2.76	2.68	2.09	1.93
	RMSE	–	4.37	4.50	3.30	2.84	2.54
	MAPE (%)	–	7.32	7.07	5.60	4.05	3.72
H = 6	MAE	–	3.17	3.39	2.87	2.66	2.83
	RMSE	–	4.56	5.07	3.44	3.6	3.72
	MAPE (%)	–	7.22	8.20	5.88	5.31	5.58

TS model's performance in extracting and simulating similar series in historical crude oil price data for prediction. The results also demonstrate the strength of LSTM in dealing with complex nonlinear time series. Second, based on the overall forecasting results, the significant difference of the performance of the machine learning models SVR and ELM from that of LSTM, demonstrates the strength of LSTM in dealing

Table 4
Single model forecasting error (WTI).

Horizon	Indicators	Snaive	SVR	ELM	ANN	LSTM	TS
H = 1	MAE	3.40	3.83	2.77	2.64	1.86	1.20
	RMSE	5.29	5.33	4.34	4.28	3.16	2.97
	MAPE (%)	7.66	9.53	6.98	6.79	4.56	3.17
H = 3	MAE	–	3.08	3.13	2.86	2.35	2.05
	RMSE	–	4.79	4.75	4.40	4.63	4.35
	MAPE (%)	–	7.85	7.65	7.10	6.05	5.27
H = 6	MAE	–	3.72	3.41	3.24	2.6	2.88
	RMSE	–	6.99	5.07	4.98	5.17	5.28
	MAPE (%)	–	10.52	8.22	8.00	7.09	7.07

with complex nonlinear time series. Third, as the Snaive model produced relatively acceptable results within the broad scope considered in this study, we see the presence of a strong periodicity in the original sequence.

In measuring the similarity between different time series, the advantage of TS is revealed in better forecasting results. For a more

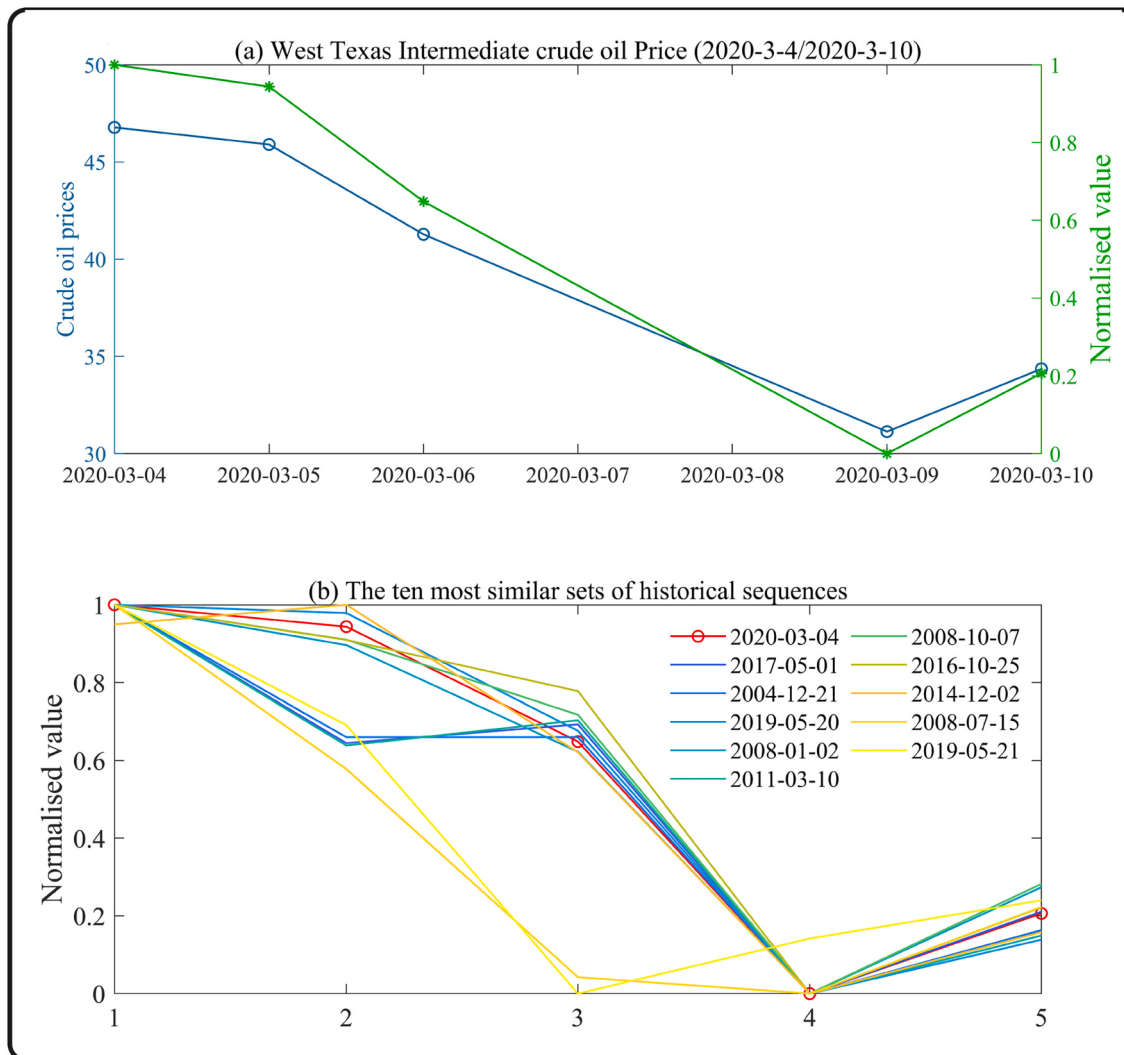


Fig. 11. Partial demonstration of trajectory similarity (fluctuation period).

intuitive representation of the interpretability of trajectory similarity, we take out a representative case. We set a time window of 5, so that the original time series can be transformed into a set of 5×1 vectors; within this set of vectors, we can obtain the ten sets of sequences that are most similar to the target vector by computing them (according to the dynamic time warping (DTW) proposed in the research). Since these ten sets of sequences are past occurrences, they have specific information about the next time point (or the next h time points), so we can use them to calculate the forecasting values corresponding to each set of sequences (through a normalization process); finally, we average the ten sets of predictions, and then perform the inverse normalization to obtain the final prediction values. Fig. 11(a) shows the WTI data for the five business days from March 4, 2020 to March 11, 2020. Fig. 11(b) shows the ten most similar sequences to this series in the historical US WTI data from which the TS model predictions were derived. The OPEC+ negotiations ended inconclusively during the chosen period, and international crude oil prices plummeted in response to a frantic sell-off. In the chart, we can see that there are similar trajectories in historical crude oil price movements, such as near May 1, 2017, and near December 21, 2004, when crude oil prices experienced similar ups and downs, affecting markets and practitioners with similar dynamics. We can thereby draw on past trends in oil prices under similar scenarios to guide future price forecasts. In addition, we provide a figure of a relatively flat period, i.e., the normal period, as shown in Fig. 12. Fig. 12(a) shows the WTI data for the five business days from January 2, 2020 to January 8,

2020. Fig. 12(b) shows the ten most similar sequences to this series in the historical US WTI data. In the two different situations, we can find similar trajectories always appearing.

Although TS has better single-model prediction performance, due to its overreliance on historical datasets and consideration of computational efficiency, it becomes unsuitable for predicting high-frequency series. With this consideration in mind, we choose LSTM as more capable of handling nonlinear time series for the prediction of high-frequency modes. In summary, to assess the predictive accuracy and robustness of the proposed approach (i.e., VMD-SE-TS/LSTM), two superior comparative models, LSTM and TS, were selected to be combined with the decomposition model. Also, to verify the effectiveness of the decomposition method (VMD) supported in this study, we chose complete integration empirical mode decomposition algorithm (CEEMDAN) as the decomposition algorithm for comparison (Torres et al., 2011). The CEEMDAN algorithm may preserve the integrity of empirical mode decomposition decomposition (EMD) and resolve the issue of reconstruction inaccuracy caused by the phenomenon of modal mixing and poor efficiency (Yeh et al., 2010; Wu and Huang, 2009). The predictive performance of all models was evaluated using the three criteria, MAE, RMSE and MAPE, over three time periods, i.e., 1, 3 and 6 time steps. Evaluation results of each criterion are shown in Tables 5–6, while the fitted curves based on one-step-ahead forecasts with comparative plots are in Figs. 13–14.

Concerning these models' forecasting errors the bolded values in the

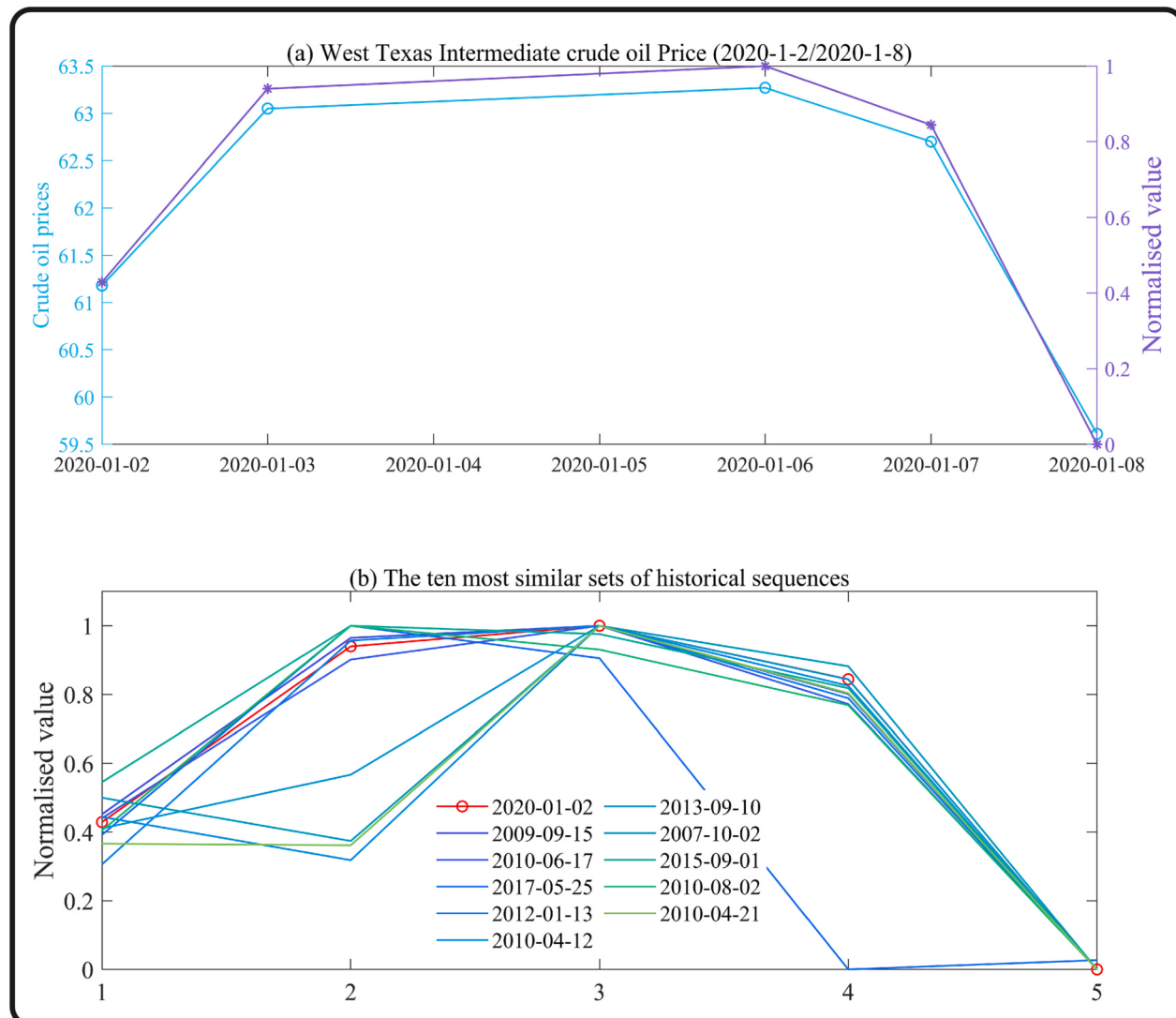


Fig. 12. Partial demonstration of trajectory similarity (normal period).

Table 5
Forecasting error and ranking of models combining decomposition algorithms (Brent).

Horizon	Indicators	TS	CEEMDAN- LSTM	CEEMDAN- TS	VMD- LSTM	VMD- TS	Hybrid approach
H = 1	MAE	1.61	1.38	1.33	1.29	1.11	0.72
	RMSE	1.97	1.87	1.78	1.76	1.52	1.01
	MAPE (%)	3.07	2.75	2.56	2.52	2.18	1.53
	Rank	6	5	4	3	2	1
H = 3	MAE	1.93	1.82	1.73	1.84	1.81	0.82
	RMSE	2.54	2.35	2.42	2.51	2.20	1.11
	MAPE (%)	3.72	3.4	3.48	3.61	3.37	1.72
	Rank	6	3	4	5	2	1
H = 6	MAE	2.83	1.94	2.22	1.66	1.73	1.39
	RMSE	3.72	2.64	2.84	2.22	2.16	1.89
	MAPE (%)	5.58	3.8	4.14	3.21	3.38	2.71
	Rank	6	4	5	2	3	1

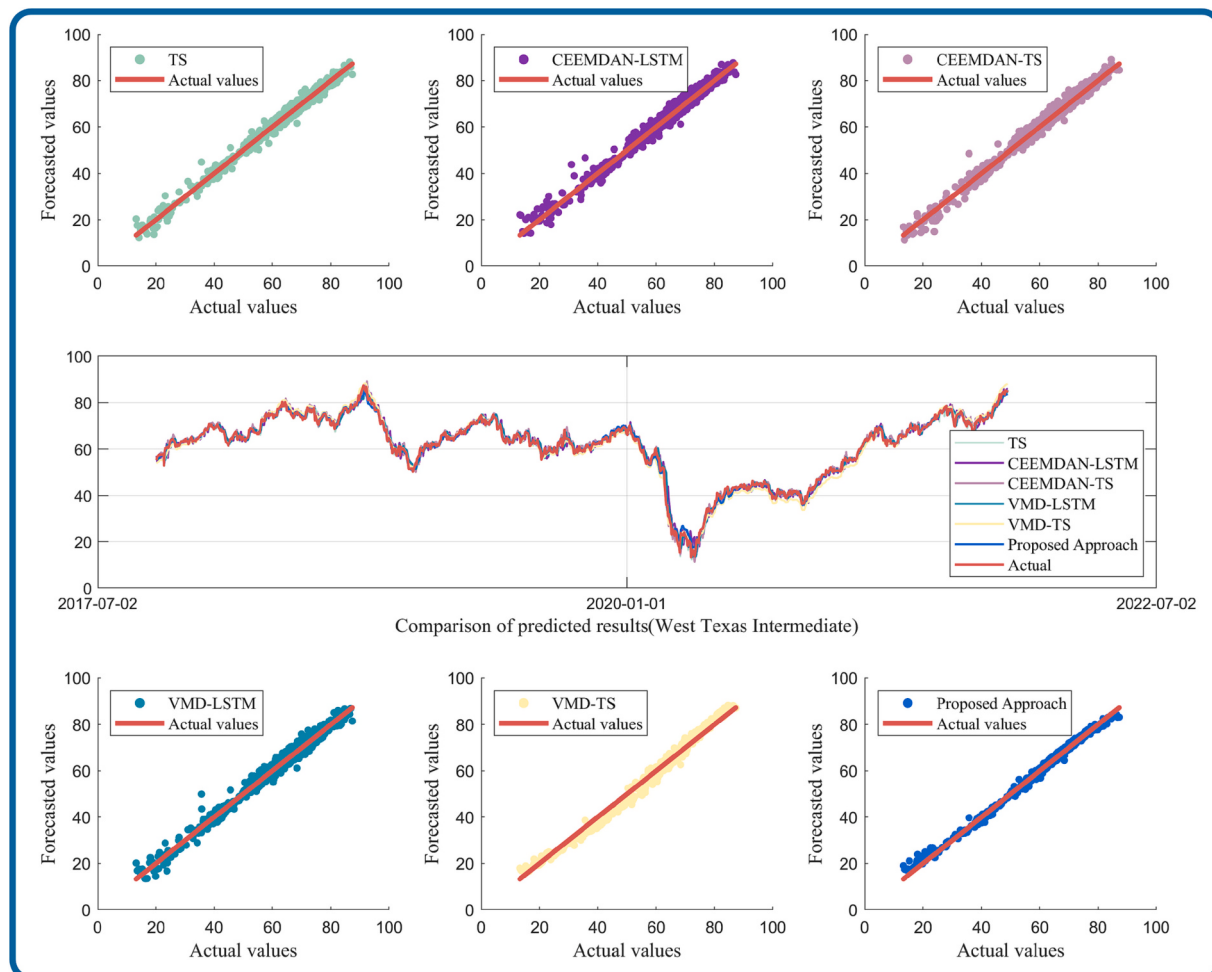
farthest right columns of Tables 5–6 represent the comparative positions of the optimum values (with the fewest mistakes). This table is instructive in three ways: The errors of models using the decomposition method are lower than those of the single-model TS. Taking Brent as an example, the MAE values for one-step ahead forecasts decreased by an average of 27.58%, and comparable findings for the other two types of time steps, each of the four hybrid models has been improved compared to the single model. After extracting the built-in modes of the original

series, the decomposition algorithm, in effect, assists the prediction model in capturing the trend of each mode, and better prediction is the result. Also, Tables 5–6 show that the proposed model's error were somewhat lower than those of the four combined models mentioned above (CEEMDAN-LSTM, CEEMDAN-TS, VMD-LSTM and VMD-TS), having an average decrease of 43.64% for the one-step forward prediction of MAE values. Because the TS and LSTM models take the best advantage of extracting information in the prediction process of low-

Table 6

Forecasting error and ranking of models combining decomposition algorithms (WTI).

Horizon	Indicators	TS	CEEMDAN-LSTM	CEEMDAN-TS	VMD-LSTM	VMD-TS	Hybrid approach
H = 1	MAE	1.20	1.1	1.07	1.07	1.15	0.63
	RMSE	2.97	2.82	2.71	2.69	2.00	1.64
	MAPE (%)	3.17	2.98	2.77	2.73	2.37	1.48
	Rank	6	5	4	3	2	1
H = 3	MAE	2.05	1.31	1.52	1.1	1.35	0.77
	RMSE	4.35	3.02	3.48	2.85	2.22	1.75
	MAPE (%)	5.27	3.43	4.05	2.94	2.89	1.73
	Rank	6	4	5	3	2	1
H = 6	MAE	2.88	1.83	1.29	1.09	1.39	1.05
	RMSE	5.28	3.59	3.05	2.71	2.41	1.93
	MAPE (%)	7.07	4.6	3.48	2.84	3.00	2.24
	Rank	6	5	4	2	3	1

**Fig. 13.** The fitting performance with comparison plots (Brent).

frequency and high-frequency modes, respectively, they perhaps integrate to obtain more accurate prediction results. A third insight from Tables 5–6 is that, though the results of the two sets of crude oil price series are not identical, the overall model performance is consistent in terms of ranking, validating the previous view that the hybrid model outperforms the single model and the proposed model achieves optimal performance.

In Figs. 13–14, the middle section depicts fitted curves for each model (including TS, CEEMDAN-LSTM, CEEMDAN-TS, VMD-LSTM, VMD-TS and VMD-SE-TS/LSTM), where red indicates actual values and blue predicted values from the proposed method. To illustrate the fit of each model, six subplots are shown in the order of TS, CEEMDAN-LSTM,

CEEMDAN-TS, VMD-LSTM, VMD-TS and VMD-SE-TS/LSTM, with the red line indicating the position of the actual values. The closer the model to the red line, the better it is. We can observe the light green scatters in the TS model are the most dispersed and furthest from the red line; the purple scatters in the CEEMDAN-LSTM model and fluorescent yellow scatters in the VMD-TS model achieve a higher level of convergence than the TS model (TS model is slightly better than the former); the blue scatters, representing the proposed approach, are almost always close to the best-fit red line. For specific details, see Figs. 13–14.

3.4.2. Statistical tests

The Wilcoxon signed rank test and the SPA test were used in this

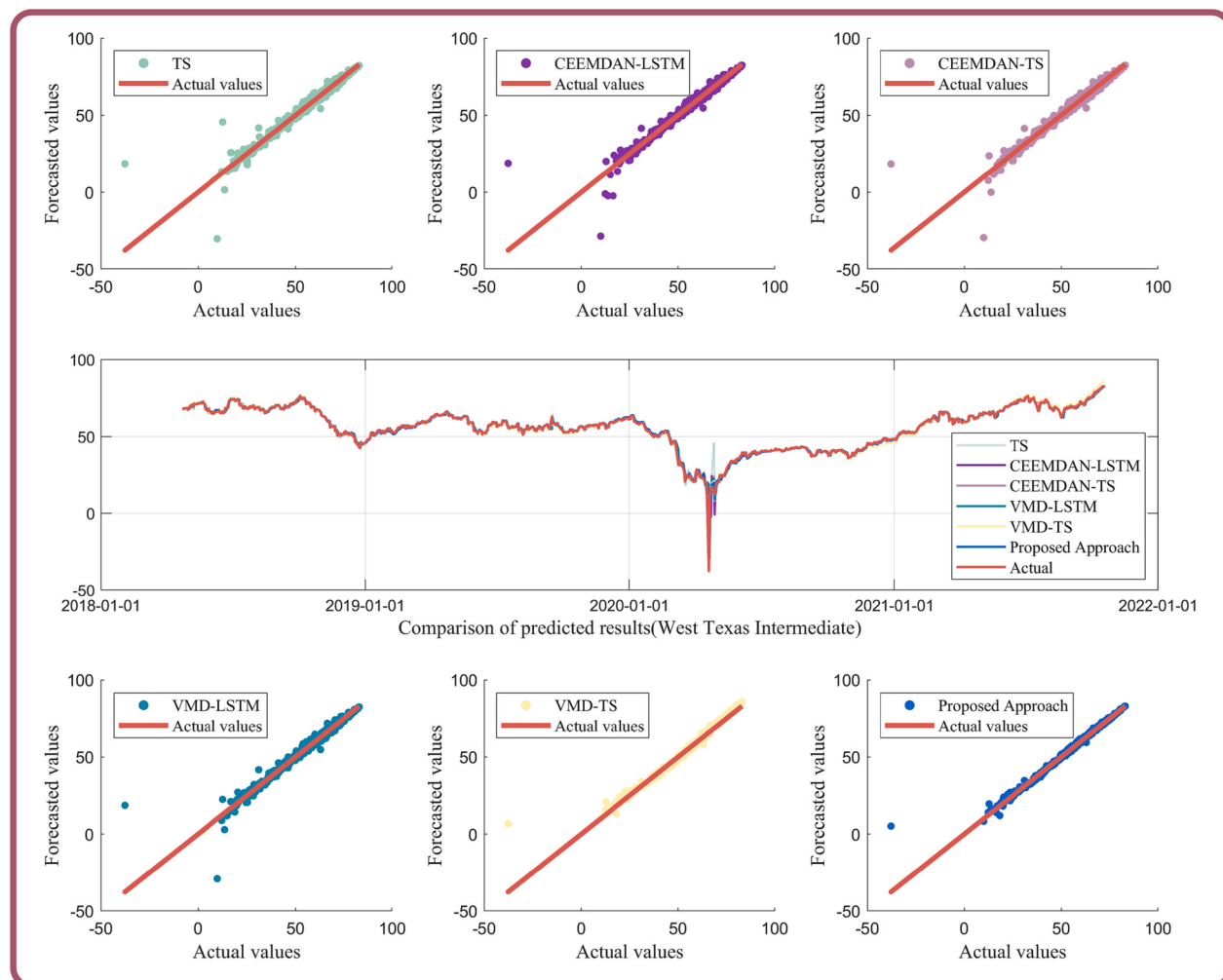


Fig. 14. The fitting performance with comparison plots (WTI).

Table 7

Results of the Wilcoxon signed rank test and the SPA test (Brent).

Panel A: The Wilcoxon signed rank test												
	Snaive	SVR	ELM	BPNN	LSTM	TS	CEEMDAN-LSTM	CEEMDAN-TS	VMD-LSTM	VMD-TS	Hybrid approach	
Snaive		0.0000	0.0000	0.0000	0.0000	0.0000	0.0000	0.0000	0.0000	0.0000	0.0000	
SVR			0.5526	0.0000	0.0000	0.0000	0.0000	0.0000	0.0000	0.0000	0.0000	
ELM				0.0018	0.0000	0.0000	0.0000	0.0000	0.0000	0.0000	0.0000	
BPNN					0.0000	0.0005	0.0000	0.0000	0.0000	0.0000	0.0000	0.0000
LSTM						0.0000	0.0000	0.0000	0.0000	0.0000	0.0000	0.0000
TS							0.0000	0.0000	0.0000	0.0000	0.0000	0.0000
CEEMDAN-LSTM								0.0436	0.0014	0.0000	0.0000	0.0000
CEEMDAN-TS									0.0000	0.0000	0.0000	0.0000
VMD-LSTM									0.0000	0.0000	0.0000	0.0000
VMD-TS										0.0000	0.0000	0.0000
Panel B: The SPA test												
	Snaive	SVR	ELM	BPNN	LSTM	TS	CEEMDAN- LSTM	CEEMDAN- TS	VMD- LSTM	VMD- TS	Hybrid approach	
Snaive		0.0000	0.0000	0.0000	0.0000	0.0000	0.0000	0.0000	0.0000	0.0000	0.0000	
SVR	1.0000		0.1263	0.0000	0.0000	0.0000	0.0000	0.0000	0.0000	0.0000	0.0000	
ELM	1.0000	0.8035		0.0000	0.0000	0.0000	0.0000	0.0000	0.0000	0.0000	0.0000	
BPNN	1.0000	1.0000	1.0000		0.0000	0.0040	0.0000	0.0000	0.0000	0.0000	0.0000	
LSTM	1.0000	1.0000	1.0000			0.0000	0.0000	0.0000	0.0000	0.0000	0.0000	
TS	1.0000	1.0000	1.0000	1.0000			0.0000	0.0000	0.0000	0.0000	0.0000	
CEEMDAN-LSTM	1.0000	1.0000	1.0000	1.0000	1.0000	1.0000		0.0541	0.0032	0.0000	0.0000	
CEEMDAN-TS	1.0000	1.0000	1.0000	1.0000	1.0000	1.0000	0.9562		0.0000	0.0000	0.0000	
VMD-LSTM	1.0000	1.0000	1.0000	1.0000	1.0000	1.0000	0.9936	1.0000		0.0000	0.0000	
VMD-TS	1.0000	1.0000	1.0000	1.0000	1.0000	1.0000	1.0000	1.0000	1.0000		0.0000	
Hybrid approach	1.0000	1.0000	1.0000	1.0000	1.0000	1.0000	1.0000	1.0000	1.0000	1.0000		

Table 8

Results of the Wilcoxon signed rank test and the SPA test (WTI).

Panel A: The Wilcoxon signed rank test											
	Snaive	SVR	ELM	BPNN	LSTM	TS	CEEMDAN-LSTM	CEEMDAN-TS	VMD-LSTM	VMD-TS	Hybrid approach
Snaive		0.0000	0.0000	0.0000	0.0000	0.0000	0.0000	0.0000	0.0000	0.0000	0.0000
SVR			0.0695	0.0000	0.0000	0.0000	0.0000	0.0000	0.0000	0.0000	0.0000
ELM				0.0033	0.0000	0.0005	0.0000	0.0000	0.0000	0.0000	0.0000
BPNN					0.0000	0.0001	0.0000	0.0000	0.0000	0.0000	0.0000
LSTM						0.0000	0.0000	0.0000	0.0000	0.0000	0.0000
TS							0.0000	0.0000	0.0000	0.0000	0.0000
CEEMDAN-LSTM								0.0000	0.0000	0.0000	0.0000
CEEMDAN-TS									0.0498	0.0000	0.0000
VMD-LSTM										0.0000	0.0000
VMD-TS											0.0000
Panel B: The SPA test											
	Snaive	SVR	ELM	BPNN	LSTM	TS	CEEMDAN-LSTM	CEEMDAN-TS	VMD-LSTM	VMD-TS	Hybrid approach
Snaive		0.9993	0.0000	0.0000	0.0000	0.0000	0.0000	0.0000	0.0000	0.0000	0.0000
SVR			0.3492	0.0000	0.0000	0.0000	0.0000	0.0000	0.0000	0.0000	0.0000
ELM				0.7026	0.2695	0.0000	0.0000	0.0000	0.0000	0.0000	0.0000
BPNN					0.7739	0.0000	0.0000	0.0000	0.0000	0.0000	0.0000
LSTM						1.0000	0.0000	0.0000	0.0000	0.0000	0.0000
TS							1.0000	0.0000	0.0000	0.0000	0.0000
CEEMDAN-LSTM								1.0000	0.0000	0.0000	0.0000
CEEMDAN-TS									0.1463	0.0000	0.0000
VMD-LSTM										0.8611	0.0000
VMD-TS											0.0000
Hybrid approach											1.0000

study to statistically evaluate the differences in the models' forecasting performance and to check the findings' robustness. Results with p -values are given in Tables 7–8. The p -value in panel A of each table indicates a significant difference between the two comparison models, and the p -value in panel B indicates whether there is a significant superiority relationship between the two comparison models. For example, in Panel A, the p -value in row 2, column 3 is 0.000, meaning the test rejects at a 99% confidence level the null hypothesis (the null hypothesis is that, there is no significant difference between SVR and Snaive models). Additionally, in Panel B, the p -value in row 2, column 3 is 0.000, indicating the test rejects the null hypothesis at a 99% confidence level (the null hypothesis is that, in forecasting performance, Snaive beats the SVR model). Combining these two tests, it can be concluded that there are significant differences between the two models, Snaive and SVR, and SVR is superior to Snaive.

Tables 7–8 statistically compare each models' forecasting performance for Brent and WTI crude oil price data. What is striking in these tables is that: (1) When VMD-SE-TS/LSTM, the approach proposed in this study, is considered the benchmark model for Panels A and B, the p -values for both tests are 0.000 and 1.000 in all cases, respectively, indicating that the proposed method significantly outperforms all other comparative models at a 99.9% confidence level. (2) CEEMDAN-LSTM, CEEMDAN-TS, VMD-LSTM and VMD-TS are statistically superior to the four single models, also confirming the efficacy of decomposing the composite forecast. (3) The performance of the six single models was also clearly demonstrated. TS was best, followed by LSTM, ANN and Snaive, while SVR and ELM fell short.

4. Conclusion

In this study, we propose a decomposition ensemble framework for the adaptive prediction of high- and low- frequency modes, i.e., VMD-SE-TS/LSTM. Specifically, we collect crude oil price data and perform VMD decomposition to provide valid and unexploited information (IMFs) for forecasting. Based on this, we use SE, an effective information evaluation tool for the adaptive separation of IMFs. Then, the data with different frequencies are predicted using models suited for each of them, i.e., low-frequency subsequences correspond to TS models with improved interpretability, and high-frequency subsequences relate to LSTM models that are better at handling complex data. Finally, by

combining the advantages of both, accurate and robust crude oil price forecasts are obtained, which can better guide the future decisions and actions of managers and practitioners.

The implications for academics and practice can be seen in the innovative forecasting framework. First, after the TS model is applied for the first time in the field of crude oil price forecasting, it produces excellent forecasting results. This will help researchers find similar phases in historical periods when processing crude oil price series, thereby assisting the ongoing research in viewing the trending and in learning from experience. Second, distinguishing multiple modes by time complexity and separately targeting high- and low- frequency data will, to some extent, provide new ideas for the crude oil price forecasting and decomposition ensemble framework, and expand the research scope. Third, crude oil market practitioners can benefit from the framework's accurate forecasts, helping them to make sound decisions, allocate resources wisely, and manage inventories effectively. Policy-makers will gain solid evidence from the framework to change policies and undertake appropriate crude oil market planning and management. Finally, since the framework is also universal, it can be used for other complex forecasting problems and for event analysis involving stocks, travel demand, and exchange rate.

Although the approach this study proposed achieved satisfactory and robust results, many shortcomings need to be refined. First, as the TS is closely related to the size of the matching set, optimization of its computational efficiency becomes more important. Second, this study could in future adopt more advanced time series prediction models for comparative evaluation, such as temporal convolutional network, and transformer. Third, the advantages recognized in this study may be better validated in a dataset where normality and crisis are handled separately. These are exciting topics that we will research in the near future.

Authors' contributions list

Mingchen Li and **Yunjie Wei** conceived of the presented idea. **Mingchen Li** developed the integrated analysis framework and performed the experiment. **Mingchen Li**, **Zishu Cheng** and **Wencan Lin** collected and analyzed the data. **Mingchen Li** and **Yunjie Wei** contributed to the interpretation of the results. **Shouyang Wang** encouraged **Mingchen Li**, **Zishu Cheng** and **Wencan Lin** to make such

a study and supervised the findings of this work. All authors provided critical feedback and helped shape the research, analysis and manuscript. All authors read and approved the manuscript.

Acknowledgements

This research work was partly supported by the National Natural Science Foundation of China under Grants No. 72171223, No. 71801213, and No. 71988101.

Appendix A. Supplementary data

Supplementary data to this article can be found online at <https://doi.org/10.1016/j.eneco.2023.106736>.

References

- Bergmeir, C., Hyndman, R.J., Benítez, J.M., 2016. Bagging exponential smoothing methods using STL decomposition and Box–Cox transformation. *Int. J. Forecast.* 32, 303–312. <https://doi.org/10.1016/j.ijforecast.2015.07.002>.
- Chai, J., Xing, L.M., Zhou, X.Y., Zhang, Z.G., Li, J.X., 2018. Forecasting the WTI crude oil price by a hybrid-refined method. *Energy Econ.* 71, 114–127. <https://doi.org/10.1016/j.eneco.2018.02.004>.
- Charles, A., Darné, O., 2017. Forecasting crude-oil market volatility: further evidence with jumps. *Energy Econ.* 67, 508–519. <https://doi.org/10.1016/j.eneco.2017.09.002>.
- Chen, C., 2004. Searching for intellectual turning points: progressive knowledge domain visualization. *Proc. Natl. Acad. Sci. U. S. A.* 101, 5303–5310. <https://doi.org/10.1073/pnas.0307513100>.
- Dehak, N., Kenny, P.J., Dehak, R., Dumouchel, P., Ouellet, P., 2011. Front-end factor analysis for speaker verification. *IEEE Trans. Audio Speech Lang. Process.* 19, 788–798. <https://doi.org/10.1109/TASL.2010.2064307>.
- Drachal, K., 2016. Forecasting spot oil price in a dynamic model averaging framework — have the determinants changed over time? *Energy Econ.* 60, 35–46. <https://doi.org/10.1016/j.eneco.2016.09.020>.
- Dragomiretskiy, K., Zosso, D., 2014. Variational mode decomposition. *IEEE Trans. Signal Process.* 62, 531–544. <https://doi.org/10.1109/TSP.2013.2288675>.
- D'Urso, P., De Giovanni, L., Massari, R., 2021. Trimmed fuzzy clustering of financial time series based on dynamic time warping. *Ann. Oper. Res.* 299, 1379–1395. <https://doi.org/10.1007/S10479-019-03284-1>.
- Ghoddisi, H., Creamer, G.G., Rafizadeh, N., 2019. Machine learning in energy economics and finance: a review. *Energy Econ.* 81, 709–727. <https://doi.org/10.1016/j.eneco.2019.05.006>.
- Godarzi, A.A., Amiri, R.M., Talaee, A., Jamasb, T., 2014. Predicting oil price movements: a dynamic artificial neural network approach. *Energy Policy* 68, 371–382. <https://doi.org/10.1016/j.enpol.2013.12.049>.
- Hansen, P.R., 2005. A test for superior predictive ability. *J. Bus. Econ. Stat.* 23, 365–380. <https://doi.org/10.1198/073500105000000063>.
- Jammazi, R., Aloui, C., 2012. Crude oil price forecasting: experimental evidence from wavelet decomposition and neural network modeling. *Energy Econ.* 34, 828–841. <https://doi.org/10.1016/j.eneco.2011.07.018>.
- Karasu, S., Altan, A., Bekiros, S., Ahmad, W., 2020. A new forecasting model with wrapper-based feature selection approach using multi-objective optimization technique for chaotic crude oil time series. *Energy* 212. <https://doi.org/10.1016/j.energy.2020.118750>.
- Kim, H., Ahn, C.R., Engelhardt, D., Lee, S.H., 2018. Application of dynamic time warping to the recognition of mixed equipment activities in cycle time measurement. *Autom. Constr.* 87, 225–234. <https://doi.org/10.1016/j.autcon.2017.12.014>.
- Lecun, Y., Bengio, Y., Hinton, G., 2015. Deep learning. *Nat.* 5217553 (521), 436–444. <https://doi.org/10.1038/nature14539>, 2015.
- Li, H., 2021. Time works well: dynamic time warping based on time weighting for time series data mining. *Inf. Sci. (Ny)*. 547, 592–608. <https://doi.org/10.1016/j.ins.2020.08.089>.
- Li, H., Bai, J., Cui, X., Li, Y., Sun, S., 2020. A new secondary decomposition-ensemble approach with cuckoo search optimization for air cargo forecasting. *Appl. Soft Comput.* 90. <https://doi.org/10.1016/j.asoc.2020.106161>.
- Li, Y., Jiang, S., Li, X., Wang, S., 2021. The role of news sentiment in oil futures returns and volatility forecasting: data-decomposition based deep learning approach. *Energy Econ.* 95, 105140. <https://doi.org/10.1016/j.eneco.2021.105140>.
- Lu, Q., Li, Y., Chai, J., Wang, S., 2020. Crude oil price analysis and forecasting: a perspective of “new triangle”. *Energy Econ.* 87, 104721. <https://doi.org/10.1016/j.eneco.2020.104721>.
- Luo, Z., Cai, X., Tanaka, K., Takiguchi, T., Kinkyo, T., Hamori, S., 2019. Can we forecast daily oil futures prices? Experimental evidence from convolutional neural networks. *J. Risk Financ. Manag.* 12. <https://doi.org/10.3390/JRFM12010009>, 2019. 9 12, 9.
- Ma, F., Zhang, Y., Huang, D., Lai, X., 2018. Forecasting oil futures price volatility: new evidence from realized range-based volatility. *Energy Econ.* 75, 400–409. <https://doi.org/10.1016/j.eneco.2018.09.006>.
- Miao, H., Ramchander, S., Wang, T., Yang, D., 2017. Influential factors in crude oil price forecasting. *Energy Econ.* 68, 77–88. <https://doi.org/10.1016/j.eneco.2017.09.010>.
- Mohammadi, H., Su, L., 2010. International evidence on crude oil price dynamics: applications of ARIMA-GARCH models. *Energy Econ.* 32, 1001–1008. <https://doi.org/10.1016/j.eneco.2010.04.009>.
- Nademi, A., Nademi, Y., 2018. Forecasting crude oil prices by a semiparametric Markov switching model: OPEC, WTI, and Brent cases. *Energy Econ.* 74, 757–766. <https://doi.org/10.1016/j.eneco.2018.06.020>.
- Pham, T.D., Yan, H., 2018. Spatial-dependence recurrence sample entropy. *Phys. A Stat. Mech. its Appl.* 494, 581–590. <https://doi.org/10.1016/j.physa.2017.12.015>.
- Qadan, M., Nama, H., 2018. Investor sentiment and the price of oil. *Energy Econ.* 69, 42–58. <https://doi.org/10.1016/j.eneco.2017.10.035>.
- Ratti, R.A., Vespiagnani, J.L., 2016. Oil prices and global factor macroeconomic variables. *Energy Econ.* 59, 198–212. <https://doi.org/10.1016/j.eneco.2016.06.002>.
- Risse, M., 2019. Combining wavelet decomposition with machine learning to forecast gold returns. *Int. J. Forecast.* 35, 601–615. <https://doi.org/10.1016/j.ijforecast.2018.11.008>.
- Tang, L., Wu, Y., Yu, L., 2018. A randomized-algorithm-based decomposition-ensemble learning methodology for energy price forecasting. *Energy* 157, 526–538. <https://doi.org/10.1016/j.energy.2018.05.146>.
- Tang, L., Zhang, C., Li, L., Wang, S., 2020. A multi-scale method for forecasting oil price with multi-factor search engine data. *Appl. Energy* 257, 114033. <https://doi.org/10.1016/j.apenergy.2019.114033>.
- Teterin, P., Brooks, R., Enders, W., 2016. Smooth volatility shifts and spillovers in U.S. crude oil and corn futures markets. *J. Empir. Financ.* 38, 22–36. <https://doi.org/10.1016/j.jempfin.2016.05.005>.
- Torres, M.E., Colominas, M.A., Schlotthauer, G., Flandrin, P., 2011. A complete ensemble empirical mode decomposition with adaptive noise. In: ICASSP, IEEE International Conference on Acoustics, Speech and Signal Processing - Proceedings, pp. 4144–4147. <https://doi.org/10.1109/ICASSP.2011.5947265>.
- Wang, Y., Wu, C., Yang, L., 2016. Forecasting crude oil market volatility: a Markov switching multifractal volatility approach. *Int. J. Forecast.* 32, 1–9. <https://doi.org/10.1016/j.ijforecast.2015.02.006>.
- Wang, Y., Liu, L., Wu, C., 2017. Forecasting the real prices of crude oil using forecast combinations over time-varying parameter models. *Energy Econ.* 66, 337–348. <https://doi.org/10.1016/j.eneco.2017.07.007>.
- Wang, J., Athanasopoulos, G., Hyndman, R.J., Wang, S., 2018a. Crude oil price forecasting based on internet concern using an extreme learning machine. *Int. J. Forecast.* 34, 665–677. <https://doi.org/10.1016/j.ijforecast.2018.03.009>.
- Wang, M., Tian, L., Zhou, P., 2018b. A novel approach for oil price forecasting based on data fluctuation network. *Energy Econ.* 71, 201–212. <https://doi.org/10.1016/j.eneco.2018.02.021>.
- Wang, J., Zhou, H., Hong, T., Li, X., Wang, S., 2020. A multi-granularity heterogeneous combination approach to crude oil price forecasting. *Energy Econ.* 91, 104790. <https://doi.org/10.1016/j.eneco.2020.104790>.
- Weng, F., Zhang, H., Yang, C., 2021. Volatility forecasting of crude oil futures based on a genetic algorithm regularization online extreme learning machine with a forgetting factor: the role of news during the COVID-19 pandemic. *Res. Policy* 73. <https://doi.org/10.1016/j.resourpol.2021.102148>.
- Wu, Z., Huang, N.E., 2009. Ensemble empirical mode decomposition: a noise-assisted data analysis method. *Adv. Adapt. Data Anal.* 1, 1–41. <https://doi.org/10.1142/S179353690900047>.
- Wu, Q., Lin, H., 2019. Daily urban air quality index forecasting based on variational mode decomposition, sample entropy and LSTM neural network. *Sustain. Cities Soc.* 50, 101657. <https://doi.org/10.1016/j.scs.2019.101657>.
- Wu, Y.X., Wu, Q.B., Zhu, J.Q., 2019. Improved EEMD-based crude oil price forecasting using LSTM networks. *Phys. A Stat. Mech. its Appl.* 516, 114–124. <https://doi.org/10.1016/j.physa.2018.09.120>.
- Xiao, Z., Xu, S., Li, T., Jiang, H., Zhang, R., Regan, A.C., Chen, H., 2020. On extracting regular travel behavior of private cars based on trajectory data analysis. *IEEE Trans. Veh. Technol.* 69, 14537–14549. <https://doi.org/10.1109/TVT.2020.3043434>.
- Xiong, T., Bao, Y., Hu, Z., 2013. Beyond one-step-ahead forecasting: evaluation of alternative multi-step-ahead forecasting models for crude oil prices. *Energy Econ.* 40, 405–415. <https://doi.org/10.1016/j.eneco.2013.07.028>.
- Yeh, J.R., Shieh, J.S., Huang, N.E., 2010. Complementary ensemble empirical mode decomposition: a novel noise enhanced data analysis method. *J. Adv. Adapt. Data Anal.* 2 (2), 135–156. <https://doi.org/10.1142/S1793536910000422>.
- Yu, L., Wang, S., Lai, K.K., 2008. Forecasting crude oil price with an EMD-based neural network ensemble learning paradigm. *Energy Econ.* 30, 2623–2635. <https://doi.org/10.1016/j.eneco.2008.05.003>.
- Yu, L., Zhao, Y., Tang, L., 2014. A compressed sensing based AI learning paradigm for crude oil price forecasting. *Energy Econ.* 46, 236–245. <https://doi.org/10.1016/j.eneco.2014.09.019>.
- Yu, L., Wang, Z., Tang, L., 2015. A decomposition-ensemble model with data-characteristic-driven reconstruction for crude oil price forecasting. *Appl. Energy* 156, 251–267. <https://doi.org/10.1016/j.apenergy.2015.07.025>.
- Yu, L., Zhao, Y., Tang, L., Yang, Z., 2019. Online big data-driven oil consumption forecasting with Google trends. *Int. J. Forecast.* 35, 213–223. <https://doi.org/10.1016/j.ijforecast.2017.11.005>.
- Zhang, X., Lai, K.K., Wang, S.Y., 2008. A new approach for crude oil price analysis based on empirical mode decomposition. *Energy Econ.* 30, 905–918. <https://doi.org/10.1016/j.eneco.2007.02.012>.
- Zhang, G., Wu, Y., Wong, K.P., Xu, Z., Dong, Z.Y., Iu, H.H.C., 2014. An advanced approach for construction of optimal wind power prediction intervals. *IEEE Trans. Power Syst.* 30 (5), 2706–2715. <https://doi.org/10.1109/TPWRS.2014.2363873>.
- Zhang, Y., Yan, B., Aasma, M., 2020. A novel deep learning framework: prediction and analysis of financial time series using CEEMD and LSTM. *Expert Syst. Appl.* 159, 113609. <https://doi.org/10.1016/j.eswa.2020.113609>.

- Zhang, C., Li, M., Sun, S., Tang, L., Wang, S., 2021. Decomposition methods for tourism demand forecasting: a comparative study. *J. Travel Res.* <https://doi.org/10.1177/00472875211036194>.
- Zhao, J., Itti, L., 2018. shapeDTW: shape dynamic time warping. *Pattern Recognit.* 74, 171–184. <https://doi.org/10.1016/J.PATCOG.2017.09.020>.
- Zhao, Y., Li, J., Yu, L., 2017. A deep learning ensemble approach for crude oil price forecasting. *Energy Econ.* 66, 9–16. <https://doi.org/10.1016/J.ENEKO.2017.05.023>.
- Zhao, L.T., Wang, Y., Guo, S.Q., Zeng, G.R., 2018. A novel method based on numerical fitting for oil price trend forecasting. *Appl. Energy* 220, 154–163. <https://doi.org/10.1016/J.APENERGY.2018.03.060>.
- Zhao, E., Du, P., Azaglo, E.Y., Wang, S., Sun, S., 2022. Forecasting daily tourism volume: a hybrid approach with CEMMDAN and multi-kernel adaptive ensemble. *Curr. Issue Tour.* 1-20 <https://doi.org/10.1080/13683500.2022.2048806>.